https://doi.org/10.1016/j.cej.2020.126692

De Novo Design of Polymers Embedded with Platinum Acetylides towards N-Type Organic Thermoelectrics

Xiaojun Yin[a], Tao Wan[a], Xin Deng[b], Yangsu Xie[b], Chunmei Gao[b], Cheng Zhong[c], Zhen Xu[d], Chengjun Pan[a], Guangming Chen[a], Wai-Yeung Wong[e], Chuluo Yang[a,*], and Lei Wang[a,*]

[a]*Shenzhen Key Laboratory of Polymer Science and Technology, College of Materials Science and Engineering, Shenzhen University, Shenzhen 518060*, China.
[b]*College of Chemistry and Chemical Engineering, Shenzhen University, Shenzhen 518060, PR China.*
[c]*Hubei Key Lab on Organic and Polymeric Optoelectronic Materials, Department of Chemistry, Wuhan University, Wuhan, 430072, P. R. China.*
[d]*School of Chemistry and Pharmaceutical Engineering, Qilu University of Technology (Shandong Academy of Sciences), Jinan, 250353, P.R. China.*
[e]*Department of Applied Biology and Chemical Technology, The Hong Kong Polytechnic University, Hung Hom, Hong Kong, China.*

E-mail addresses: wl@szu.edu.cn (L. Wang), clyang@szu.edu.cn (C. Yang),

Keywords: platinum acetylides, thermoelectric, Soret effect, interfacial engineering, Seebeck coefficient

Abstract

Essential task to improve the performance of n-type organic thermoelectric (TE) materials still remains great challenge due to the electron trapping and inefficient n-doping. Conducting polymers with dual electronic-ionic transport are promising for TE generators owing to their potential of both large thermoelectric responses (S) and favorable conductivities (σ). However, current progresses are mainly limited to the scanty available p-type polyelectrolytes with inferior electrical properties, which restrict the breakthrough of TE devices. Herein, three π-conjugated polymers with or without the incorporation of platinum acetylides are elaborately designed. Remarkably, the embedded platinum acetylides can effectively sharpen their

density of states nearby the Fermi levels as well as strengthening their through-bond coupling among the metal *d*-orbitals and the neighboring π-orbitals synchronously. Meanwhile, a simple interfacial modification by using trifluoromethanesulfonic acid is introduced to offer them dual electronic-ionic transport feature. Therefore, a remarkably high *S* of over -3150 μV K^{-1} and an enhanced conductivity of 17.1 S m^{-1} can be achieved by P(TBT-Pt), which is significantly superior to the P(TBTC6) without platinum acetylides. In addition, all these platinum acetylenes exhibit a low κ of around 0.5 W m^{-1} K^{-1} and thus enabling a considerable ZT value of 2.83×10^{-2} upon the optimal power factors of 47.4 μW m^{-1} K^{-2}.

1. Introduction

Thermoelectric (TE) generators that can harvest energy from temperature gradients through either the Seebeek effect and/or the Soret effect have garnered extensive attention due to their potential for recovering electrical energy from otherwise wasted heat [1-6]. In the pursuit of higher TE conversion, efforts have been devoted to bolstering both the Seebeck coefficient (S) and conductivity (σ), while restraining the thermal conductivity (κ) of the materials, since the performance of the material is determined by the dimensionless figure of merit ($ZT = S^2\sigma T/\kappa$, wherein T represents the absolute temperature) [7-11]. Recently, organic semiconductors (OSCs) adapted for TE applications have been becoming more attractive for their unique properties, such as having mechanical flexibility, being inexpensive, being non-toxic, and possessing scalable processing methods [12-19]. Owing to the intrinsically low κ of OSCs, the power factors ($PFs = S^2\sigma$) are the parameters that are left to optimize the TE performances [20-25]. Nevertheless, it can be difficult to overcome the interplay between the S and the σ according to the Mahan-Sofo theory [26-32], i.e., a high S value is almost always associated with a low σ value for typical OSCs and vice versa [33-36]. Such as Di et al. reporting a high S of -1215 ± 139 μV K^{-1} (A-DCV-DPPTT) with σ lower than 0.1 S m^{-1} [37], while Pei et al. achieving a high σ approach 1400 S m^{-1} but a significantly decreased S around

-100 μV K^{-1} (FBDPPV) [38]. Frustratingly, while chemical doping is all but required to enhance the σ for power factors (PFs) optimization [39-41], the increased electron concentration sharply decreases the *S* values, fighting against the ultimate goal of high figures of merit [28, 42]. Therefore, strategies to equilibrate these parameters are crucial.

Ionic thermoelectric effects relating polyelectrolytes can readily produce large thermopower (always several orders of magnitude higher than electronic conductors) whereby Soret effect [43-48], which enable a valid strategy to improve the performances of the TE conversion. However, the low electrical conductivity discourage most pursuers in adapt to the TE applications [49, 50]. Utilizing both ionic and electronical conductivity to optimize their TE behaviors is very promising [51-53]. Unfortunately, current progress on mixed ionic-electronic semiconductors are mainly limited to the classical p-type poly(3,4-ethylenedioxythiophene):poly(styrenesulfonate) (PEDOT:PSS) architectures [36, 54], and the performances as well as mechanisms are remaining to be clarify [51-53]. It should be noted that despite no direct current conductivity can be extracted from the ionic conductors-based TE devices, the conversion of heat-to-electricity can be realized by building an intermediate capacitors [55]. Therefore, imperative efforts to develop advanced conductive ionic polymers (especially for n-type) as well as understanding the essential effect between the ionic and electronic Seebeck are worthwhile. Alternative strategy with the concept of density of states (DOS) engineering by incorporating a heavy metal atom (e.g., platinum) into the π-conjugated system may offer an effective approach to generate satisfactory ionic TE materials [56]. Since the strong overlap between the platinum sp_x orbitals and σp_x orbitals of the π-conjugated ligand leads to localized σ bonding [57], sharpening their DOS nearby the Fermi level (E_F) of the polymers [58]. Additionally, the hybridization between the platinum dπ orbitals and the ligand pπ orbitals results in π-conjugation enhancement, ensuring a feasible channel for charge carrier transporting [59].

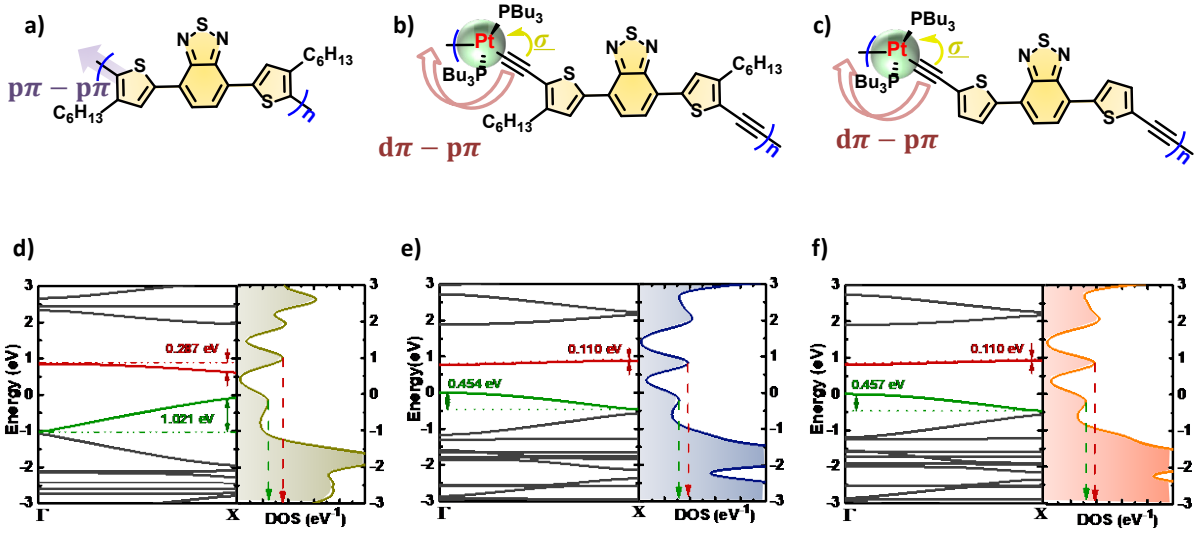

Scheme 1. Chemical structure, band structure (with the valence band was defined as 0), and partial DOS of the polymers, a)/d) for P(TBTC6), b)/e) for P(TBTC6-Pt), and c)/f) for P(TBT-Pt).

In this work, two platinum acetylenes-embedded π-conjugated polymers, namely P(TBT-Pt) and P(TBTC6-Pt) (**Scheme 1**), were elaborately designed for TE application. Meanwhile, homologous polymer of P(TBTC6) without platinum acetylides was synthesized in parallel. Density functional theory (DFT) calculation results verified that the incorporation of platinum acetylenes into the π-conjugated polymers could effectively sharpen their DOS nearby the E_{FS}. To realize dual electronic-ionic transport feature, interfacial engineering towards these polymer films was carried out by means of surface protonation using trifluoromethanesulfonic acid (TFSA). Notably, the anion-induced electron transfer between the $CF_3SO_3^-$ anions and the ionized π-acidic backbones enables an n-type self-doping (**Scheme S2**) [60, 61], which contribute to the enhancement of electronic conductivity. Moreover, direct evidence of the anion (CF_3SO_3) migration under the temperature gradient can be observed (**Figure 1e**), which could offer not only additional ionic conductivity but also S enhancement because of the higher energy-carrier-nature of the ions than the electrons [62-64]. Therefore, a remarkably high S_{mix} of -2905.5 ± 249.0 μV K^{-1} and a high σ_{mix} of 15.2 ± 1.9 S m^{-1} can be achieved by P(TBT-Pt) under the ambient condition, which are significantly superior to the model

molecules without platinum acetylenes. As expected, all these platinum acetylenes possess a low κ of around 0.5 W m^{-1} K^{-1} and thus enabling a considerable ZT_{mix} value of 2.83 × 10^{-2} upon their optimized PF_{mix} of 43.2 ±4.2 μW m^{-1} K^{-2}. The time-dependent open circuit voltage measurements of theses modified thin-films confirmed the dual contribution of electronic and ionic in promoting the TE performances. In addition, the energy dispersive spectrometer (EDS) images and the X-ray photoelectron spectroscopy (XPS) measurements provided the direct evidence to illuminate the essential mechanism of mixed electronic-ionic semiconductors in contributing to their TE parameters.

2. Results and discussion

2.1 Concepts and Theoretical calculations

To achieve both high *S* and σ of the TE films, a primary high *S* and favorable charge transfer ability of the π-conjugated backbone is essential. The rationality of manipulating the *S* by means of DOS engineering is based on the Mahan-Sofo theory [65], which can be understood from the Mott's relation (**Equation 1**), wherein k_B is the Boltzmann constant, n is the carrier concentration, μ represents the carrier mobility, and E_F stands for the Fermi energy. Notably, either by introducing the scattering mechanisms to increase the energy-dependence of μ(E) or increasing the energy-dependence of n(E) caused by a local increase of the DOS function are beneficial for promoting the *S* values. Therefore, a strongly energy-dependent DOS is critical for enhancing *S*.

$$S = -\frac{\pi^2 k_B}{3e} k_B T \left\{ \frac{1}{n} \frac{dn(E)}{dE} + \frac{1}{\mu} \frac{d\mu(E)}{dE} \right\}_{E=E_F} \qquad (1)$$

To verify our initial concept that the embedded platinum acetylides among the conjugated polymer chain will be beneficial for *S* enhancement, we performed first-principles density functional theory (DFT) calculations of the electronic DOS and band structure using DMol3

program [66]. The calculation level is PBE/DNP with DFT semi-core pseudopots on heavy atom. As **Scheme 1** shows, in comparison with the model molecules of P(TBTC6), the insertion of platinum acetylides could significantly decrease the width of both valence bands (e.g. from 1.021 to 0.454 eV) and conduction bands (e.g. from 0.287 to 0.110 eV), and then sharpen their DOS simultaneously (**Scheme 1**). Notably, the sharp increase of DOS nearby the E_{FS} is favorable for enhancing the *S*, which selective restrains the transportation of low energy carriers. Therefore, a higher *S* can be predictably achieved on both P(TBT-Pt) and P(TBTC6-Pt) than P(TBTC6) when associated to the equivalent carrier concentration. In addition, the extended π-delocalization along the polymer's main chain can be maintained *via* dπ(Pt)-pπ(C) orbital overlap (**Scheme 1**), which may provide an additional channel to improve their *σ*.

2.2 Thermoelectric and Electric properties

To evaluate the TE performances of these organic thin-films, their Seebeck coefficients and electrical conductivities were measured. Initially, interfacial engineering towards achieving dual electronic-ionic transport of the films by means of surface protonation using TFSA were carried out. Remarkably, all these samples exhibited ultra-high S_{mix} over -1000 μV K^{-1} (**Figure 1a**), which may presumably due to the key contribution of $CF_3SO_3^-$ anions whereby Soret effect, since the ionic migration mechanism beneficial for high S_{mix} derive from their higher energy-carrier nature than electron [62]. Correspondingly, the EDS measurements of P(TBT-Pt) under a certain temperature gradient give a direct view of anions ($CF_3SO_3^-$) migration to support this standpoint (**Figure 1e**). Notably, all the three compounds showed a monotonically increasing S_{mix} with the TFSA concentration range from 4.0 to 6.0 mol/L, which can mainly be attributable to the gradually increased $CF_3SO_3^-$ contents at the surfaces (**Figure S3**). However, the significantly decreasing of S_{mix} from 6.0 to 8.0 mol/L may presumably due to the increasing of carrier concentration. The highest S_{mix} of -2905.5 ± 249.0 μV K^{-1} was achieved by P(TBT-Pt), which was one of the best results for n-type organic TE

materials. As **Figure 1b** displayed, the σ_{mix} of these thin-films was gradually improved with the increase of TFSA concentration, and the highest σ_{mix} of 15.2 ± 1.9 S m^{-1} was achieved by P(TBT-Pt) at 8.0 mol/L. Notably, the significantly enhanced σ_{mix} could be not only attributable to the increased contents of $CF_3SO_3^-$ anions (**Figure S3**), but also the gradually enhanced anion radical concentrations at the surfaces (**Figure 1d**). Wherein, the formation of anion radicals may stem from the anion-induced electron transfer between the $CF_3SO_3^-$ anions and the protonated π-acidic diazosulfide moieties (**Scheme S2**) that feature an identifiable n-type self-doping at the surface (**Figure 1d**) [61]. In addition, the n-type doping behavior can also be confirmed by the following XPS results. Interestingly, in comparison with the P(TBTC6), despite the P(TBTC6-Pt) possess a sharper increased DOS nearby the E_F, the *S*s of P(TBTC6) were superior to P(TBTC6-Pt) regardless of the TFSA concentration (**Figure 1a**), which may be due to the dual electronic-ionic transport feature of the materials. Especially, the σ_{mix} of P(TBTC6-Pt) was significantly higher than P(TBTC6) reflecting a higher carrier concentration of the former than the latter, which may lower the S_{mix} of P(TBTC6-Pt). Even so, molecular design strategy with the incorporation of platinum acetylides can effectively improve their intrinsic *S*s, which is beneficial for scattering the low energy polarons and thus ensuring a both high S_{mix} and σ_{mix} for mixed ionic-electronic TE materials.

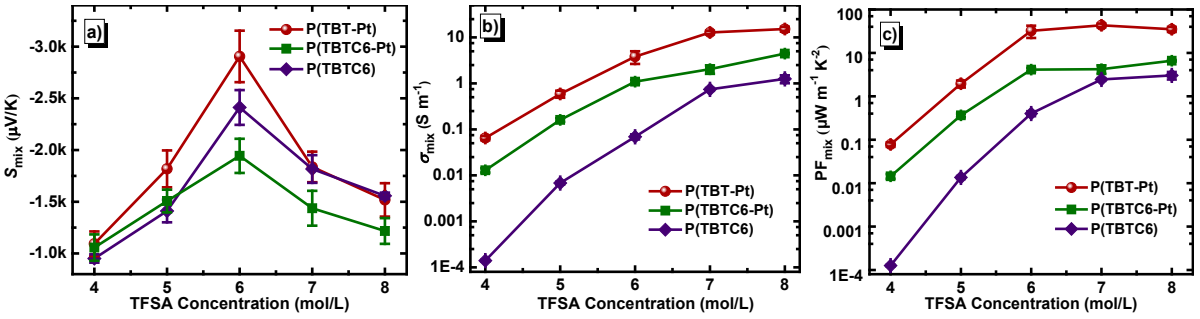

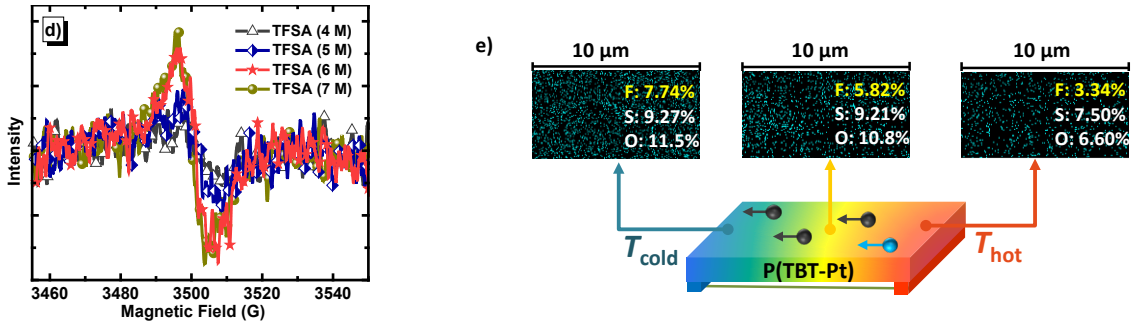

Figure 1. The a) σ_{mix}, b) S_{mix}, and c) PF_{mix} values of these samples treated with different TFSA concentration. d) The EPR spectra of the P(TBTC6-Pt) films treated with different TFSA concentrations. e) The EDS images of the F, S and O percentages of P(TBT-Pt) (treated with 7.0 mol/L TFSA) under a temperature gradient of 10 ºC (To prevent the back-diffusion of ions after the removing of temperature-gradient, the pristine film was timely cut into small perpendicular to the thermal diffusion direction).

To distinguish the contribution of ionic and electronic conductivity, time-dependent open circuit voltage (V_{oc}) of these thin-films with uniform TFSA (8 mol/L) treatment were measured. A temperature gradient of 10 ºC at 60% RH was applied between the two electrodes of the samples. As **Figure 2a** and **2b** shown, both P(TBTC6-Pt) and P(TBT-Pt) exhibited a typical ionic-electronic mixed semiconductor behaviors, i.e., the V_{oc} rapid increase up to a maximum value after a temperature gradient is applied, and then settles to a minimum value relating to the V_{oc} of the electronic charge carriers. Noticeably, the time-dependent V_{oc} of P(TBTC6) were measured in parallel, whereas no valid data can be collected due to the awful conductivity. In the meanwhile, the time-depended load current of P(TBTC6-Pt) and P(TBT-Pt) were collected. The calculated integral area of P(TBT-Pt) was significantly larger than P(TBTC6-Pt) (*ca.* 3:2, **Figure 2c**), which indicated a stronger concentration of $CF_3SO_3^-$ of the former than the latter that in line with the EDS results. **Figure 2d** revealed the σ_{mix}s as a function of the relative humidity (% RH) of the aforementioned films. Notably, all these three samples exhibited an intense RH dependence σ_{mix} throughout the entire RH range, which indicated the both contribution of electron and ion diffusion [53].

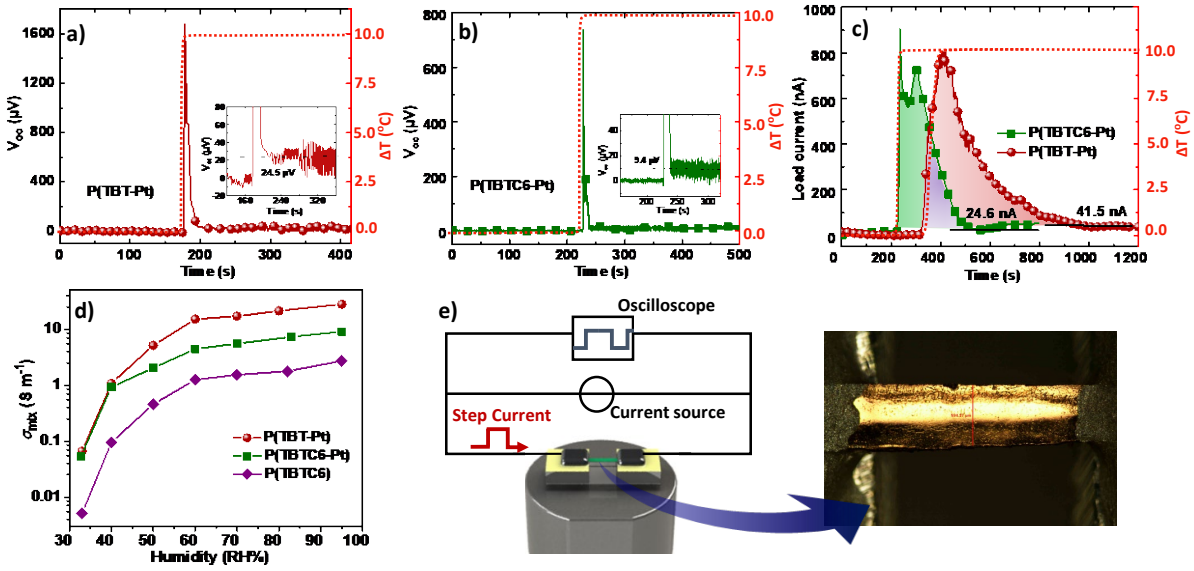

Figure 2. Time-dependent V_{oc} for a) P(TBT-Pt) and b) P(TBTC6-Pt), and c) the time-dependent load current for these two platinum acetylides, and d) the σs of these thin-films at different humidity (RH%), and e) the schematic of TET technique.

Table 1. thermoelectric data (in-plane) of these polymers modified with different TFSA concentration.

CTFSA [mol/L]	P(TBTC6)			P(TBTC6-Pt)			P(TBT-Pt)		
	S_{mix} [μV K^{-1}]	σ_{mix} [S m^{-1}]	PF_{mix} [μW m^{-1} K^{-2}]	S_{mix} [μV K^{-1}]	σ_{mix} [S m^{-1}]	PF_{mix} [μW m^{-1} K^{-2}]	S_{mix} [μV K^{-1}]	σ_{mix} [S m^{-1}]	PF_{mix} [μW m^{-1} K^{-2}]
4.0	-951.05 ± 40.2	1.4×10^{-4} ± 0.6×10^{-5}	1.3×10^{-4} ± 0.6×10^{-5}	-1057.0 ± 127.3	1.3×10^{-2} ± 0.2×10^{-2}	1.4×10^{-2} ± 0.2×10^{-2}	-1093.6 ± 118.8	6.5×10^{-2} ± 0.7×10^{-2}	7.8 × 10-2 ± 0.9 × 10-2
5.0	-1410.3 ± 109.4	6.8×10^{-3} ± 0.5×10^{-3}	1.4×10^{-2} ± 0.1×10^{-2}	-1507.0 ± 109.3	1.6×10^{-1} ± 0.2×10^{-1}	3.7×10^{-1} ± 0.4×10^{-1}	-1817.9 ± 178.3	5.9×10^{-1} ± 1.0×10^{-1}	2.0 ± 0.4
6.0	**-2411.7 ± 167.9**	6.9×10^{-2} ± 0.9×10^{-2}	4.0×10^{-1} ± 0.5×10^{-1}	**-1943.8 ± 165.3**	1.1 ± 0.1	4.1 ± 0.4	**-2905.5 ± 249.0**	3.8 ± 1.2	32.3 ± 10.2
7.0	-1816.9 ± 134.1	7.4×10^{-1} ± 0.5×10^{-1}	2.4 ± 0.2	-1436.9 ± 168.4	2.1 ± 0.4	4.2 ± 0.9	-1836.5 ± 148.0	12.8 ± 1.1	**43.2 ± 4.2**
8.0	-1557.2 ± 30.7	**1.3 ± 0.3**	**3.1 ± 0.6**	-1217.2 ± 124.2	**4.5 ± 0.2**	**6.6 ± 0.3**	-1517.9 ± 161.6	**15.2 ± 1.9**	35.0 ± 4.7

Owing to the high S_{mix} and satisfactory σ_{mix} of these platinum acetylenes, a high PF_{mix} of 6.6 ± 0.3 μW m^{-1} K^{-2} can be achieved by P(TBTC6-Pt), especially for P(TBT-Pt) (43.2 ± 4.2 μW m^{-1} K^{-2}), which was significantly superior to the model molecule of P(TBTC6) (3.1 ± 0.6 μW m^{-1} K^{-2}) (**Table 1**). To assess the ZT values of these optimized TE films, their thermal conductivities (in-plane) were measured by means of transient electro-thermal (TET)

technique. **Figure 2e** showed the schematic of experimental set-up and the details were described in the supporting information part. Unfortunately, no valid κ value for P(TBTC6) can be obtained in this manner. On the other hand, low κ_{mix}s of 0.50 and 0.51 W m^{-1} K^{-1} can be realized by P(TBT-Pt) and P(TBTC6-Pt), respectively. Therefore, the optimized ZT_{mix} values can be calculated as 2.83×10^{-2} and 4.03×10^{-3} for P(TBT-Pt) and P(TBTC6-Pt), respectively, which were among the best results for dual electronic-ionic conductive TE materials.

2.3 Surface Morphology and EDS Studies

In order to distinguish the relationships between surface morphology and TE behaviors, scanning electron microscopy (SEM) and atomic force microscope (AFM) measurements were performed. As **Figure 3** and **S4** shows, all these polymer thin-films exhibited gradually increased surface inhomogeneity with the increase of TFSA concentration in contrast to the initially homogeneous surfaces. It is worth noting that the increased surface inhomogeneity related to the ionization ratios of the polymers at the surfaces, which can be confirmed from the EDS images of the F contents (**Figure S3**), i.e., the F contents gradually increased with the TFSA solution from 4.0 mol/L to 8.0 mol/L. The AFM images of both P(TBT-Pt) and P(TBTC6-Pt) treated with or without 7.0 mol/L TFSA are displayed in **Figure 3e-3h**. In comparison with the pristine surface (**Figure 3e/3g**), significantly enhanced surface roughness can be observed after the treatment of TFSA solution (**Figure 3f/3h**) that in line with the SEM results. On the other hand, the dramatically reduced interface contact angle between the polymer surface and the water drop (**Figure 3i, 3j** and **S5**) indicate the enhanced hydrophilicity of the polymer surfaces after the modification of TFSA, which can be attributed to the surface protonation. Notably, the increased surface hydrophilicity and inhomogeneity provide an expanded contact area for the adhering of ions, which is beneficial for S and σ optimization. Interestingly, all these TE films remaining macroscopic smooth

surfaces and self-standing nature regardless of the TFSA treatment render them potential for wearable or scalable applications (**Figure 3k**).

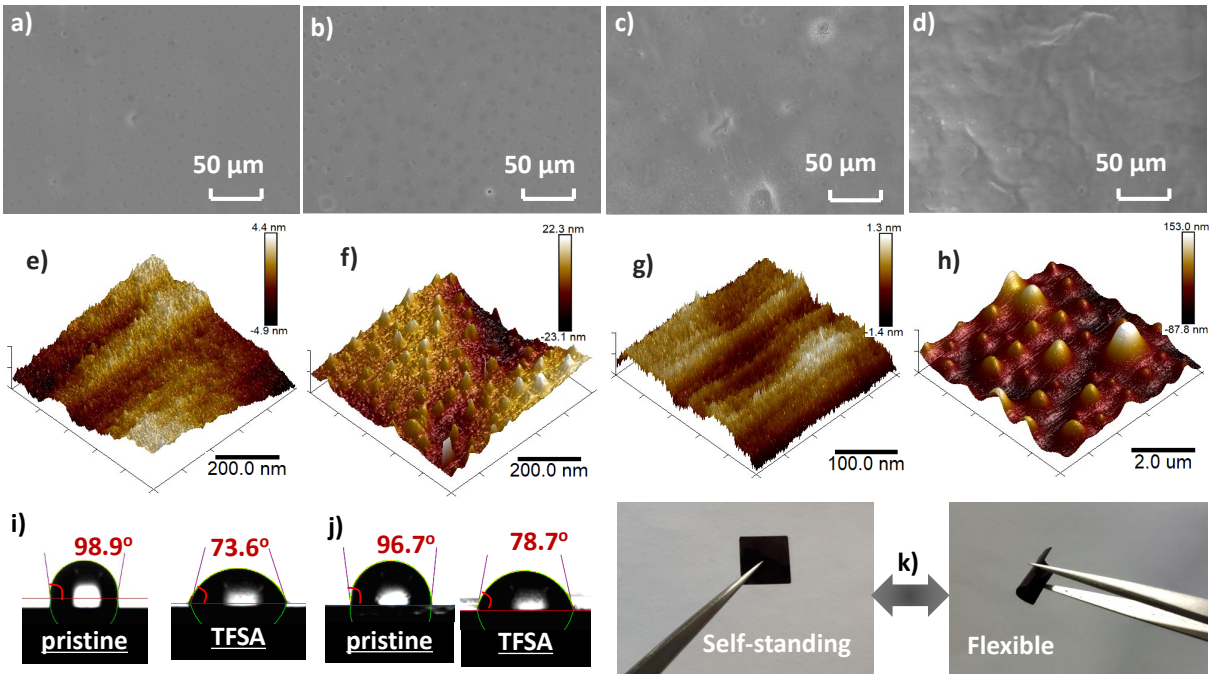

Figure 3. SEM images of the P(TBT-Pt) films treated with a) 0.0 mol/L, b) 4.0 mol/L, c) 6.0 mol/L, d) 8.0 mol/L TFSA. The AFM images of the pristine e)/g) and modified with 7.0 mol/L TFSA solutions f)/h) for P(TBT-Pt)/P(TBTC6-Pt), respectively. Interface contact angles of the i) P(TBT-Pt) and j) P(TBTC6-Pt). k) the flexibility of the free-standing TE films.

2.4 X-ray diffraction Characterization

X-ray diffraction (XRD) measurements were performed to investigate the packing properties of these films with or without interfacial modification. As **Figure S6** shows, both the P(TBT-Pt) and P(TBTC6-Pt) films exhibited a strong primary diffraction peak at $2\theta \simeq 26.6°$, which revealed a *d*-spacing of 3.35 Å, corresponding to the π-π stacking distance. Notably, the intensity of the peaks (26.6°) diminished with the concomitant increase of TFSA concentration, which may due to the surface protonation. However, in comparison with the P(TBT-Pt) films, the P(TBTC6-Pt) displayed a more corrosion stability towards TFSA, which may attributed to the more compact film surfaces of the latter than the former (**Figure S8**).

Nevertheless, the reduced π-π stacking among the polymer salts at the surface may adverse to the electron transport, but the anion-induced n-doping promoted the radical concentration in the meanwhile, and thus high σ_{mix} can be achieved.

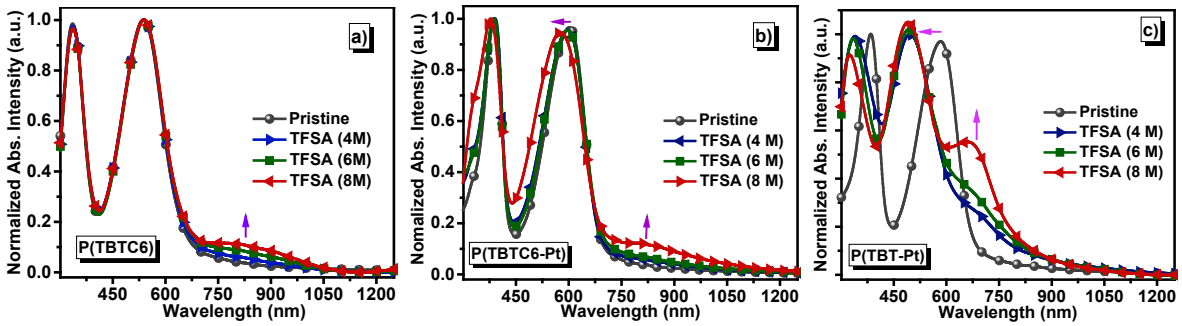

Figure 4. UV-Vis-NIR spectra of these polymer thin-films treated with various TFSA concentrations, a) for P(TBTC6), b) for P(TBTC6-Pt) and c) for P(TBT-Pt).

2.5 Photophysical Properties

To discuss the effects of the embedded platinum and interfacial modification on regulating the opto-electronic properties of the polymers, their absorption spectra were characterized. In comparison with the monomer, the absorption peaks of the polymers were remarkably red-shifted, indicating that an increase in π-conjugation from dπ(Pt)-pπ(C) orbital overlap (**Figure S7**). Meanwhile, the thin film UV-Vis-NIR absorption spectra of these platinum acetylides, with or without TFSA treatment were measured. As shown in **Figure 4**, all the pristine films typically exhibited two absorption bands, wherein the high-energy band (385 nm) is assigned to the π-π* transition of the conjugated backbones and the low-energy band (590 nm) is attributed to the charge transfer (CT) transition.[59] Noticeably, the new absorption peaks emerged at around 700~800 nm with the concomitant increase of TFSA concentration (**Figure 4c**), presumably due to the protonation of diazosulfide moieties that result in enhancing CT transition from thiophene units to diazosulfide salts. Moreover, an unconspicuous tailing

absorption band emerged at around 800 nm and extending far into the near-infrared region (**Figure 4a** and **4b**), which may ascribed to the polaronic transitions from n-type self-doping.

2.6 XPS and FT-IR Spectroscopic Characterization

To understand the essential mechanism behind the improvement of the TE performances upon interfacial engineering, surface changes involving the valence states of both the elements and functional groups were characterized by XPS and FT-IR analyses, respectively. As **Figure 5** and **S9** revealed, all these peaks (e.g., C 1s) were gradually shifted to the higher binding energy regions upon the increase of TFSA concentration corresponding to the rise of E_Fs (i.e., n-type doping), since the binding energy was estimated with respect to the E_Fs. The surface protonation process for diazosulfide moieties can be verified by the N 1s and the FT-IR spectra. As **Figure 5b** displays, the N 1s energy level splits into two peaks, with the primary peaks at around 399 eV assigned to the amine groups of diazosulfide and the new emerging peaks at around 402 ~ 406 eV assigned to the protonated diazosulfide.[60, 61] Correspondingly, a new absorption band at the 3446 cm^{-1} region revealed the existence of N^+–H covalent bond (**Figure 5e**). **Figure 5c** exhibits the S 2p spectra of the P(TBT-Pt) films. The gradually enhanced peaks at the 170 eV region should be attributed to the increased concentration of $CF_3SO_3^-$, which was in line with the FT-IR spectra (the new absorption bands emerging at 1258, 1174, 1024 cm^{-1} in **Figure 5e** correspond to the asymmetric stretching of SO_3 groups). Interestingly, the FT-IR absorption spectra of these films at 2081 cm^{-1} (assigning to the C≡C stretching vibration) significantly decreased with the concurrent increase of the 1640 cm^{-1} peaks (corresponding to the C=C stretching), which may due to the conversion of acetenyl to ethenyl with the presence of TFSA. Noticeably, the conversion from C≡C to C=C not only extends the effective π-conjugation length, but also enables a more planer structure for molecular packing, which is beneficial for charge transport.

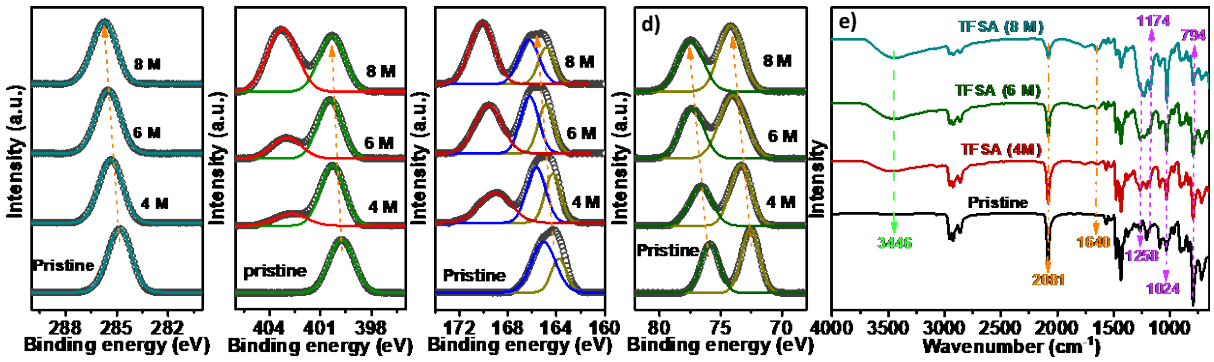

Figure 5. X-ray photoelectron spectra of the a) C 1s, b) N 1s, c) S 2p, and d) Pt 4f for P(TBT-Pt), and the FT-IR spectra of P(TBT-Pt) films treated with different concentrations of TFSA.

3. Conclusion

In conclusion, two new platinum acetylenes-embedded π-conjugated polymers with the concept of DOS engineering nearby the vicinity of their E_{FS} were meticulously designed for TE applications. Meanwhile, a simple interfacial modification was applied to these thin-films and enabling dual electronic-ionic transport feature to improve their TE performances. Significant evidence of anions diffusion along with the temperature gradient can be observed from the EDS images, and the n-type self-doping can be reflected from either XPS or EPR spectra, which provided a perspective to understand the essential of interfacial engineering-inspired TE performance optimization. Thus, an ultra-high S of over -3150 μV K^{-1} and a favorable σ of over 17.1 S m^{-1} can be realized by P(TBT-Pt), which result in a superior PF up to 47.4 μW m^{-1} K^{-2} among the N-type organic thermoelectrics. Noticeably, molecule design strategy by incorporating heavy metal atoms into the π-conjugated backbones and subsequent interfacial engineering using simple surface protonation provided an effective approach to establish advanced TE materials. It is also worth mentioning that the self-standing TE films involved in this work were fabricated by a sample drop-casting procedure with an active area over 1 cm^2 and a thickness over 10 μm, both of which enable a more capacious possibility for large-scale and flexible/wearable applications.

4. Materials and methods

Materials Synthesis: TE materials of P(TBTC6), P(TBTC6-Pt) and P(TBT-Pt) were prepared following the previously methods with some minor improvements, and the details were presented in the supporting information part.

Film Preparation and Interfacial Modification: The thin films of these polymers were prepared by drop-casting from chlorobenzene solutions on a horizontal glass plate. Firstly, P(TBTC6), P(TBTC6-Pt) or P(TBT-Pt) in chlorobenzene solution (20 mg/mL) were sonicated for 30 min. The glass substrates (10 mm × 10 mm) were cleaning using ultra sonication in acetone, deionized water, isopropanol and methanol successively, and then dried under vacuum. Then, the chlorobenzene solutions were dropped on the cleaned glass substrates carefully to form initial thin-films via volatilizing solvent. The different concentrations of TFSA solutions (4.0 ~ 8.0 mol/L) were diluted from pure TFSA with deionized water. Afterwards, surface protonation of these thin-films were carried out in corresponding TFSA solutions for appropriate times (about 4 h), and then promptly drying with high pressure nitrogen flow.

Electrical and Thermal Characterization: The conductivities, V_{oc}, and load currents of these films were collected by using a semiconductor parameter analyzer (Keithley 4200-SCS). The Seebeck coefficients were measured using thin-film thermoelectric parameter test system (MRS-3, MRS JouleYacht China) under ambient condition (RH, 60%). To adjust the *S* values of the system, a standard nickel sample was repeatedly measured (at room temperature) as a reference initially. The obtained value of -16 ± 0.3 μV K^{-1} was coincided with the reported value of -15 μV K^{-1}.[67] An average of four samples was tested to determine the TE performances for each concentration loading. The κs of these self-standing films were measured using a home-built setup (see details in the Supporting Information).

Acknowledgements

X. Yin and T. Wan contribution equally to this work. We gratefully acknowledge the financial support from the National Natural Science Foundation of China (Project Nos. 51773118, and 51803124), Shenzhen Science and Technology Research Grant (JCYJ20170818143831242, JCYJ20170818093417096).

Declarations of interest

None.

Appendix A. Supporting information

Supplementary data associated with this article can be found in the online version.

References

[1] X. Su, P. Wei, H. Li, W. Liu, Y. Yan, P. Li, C. Su, C. Xie, W. Zhao, P. Zhai, Q. Zhang, X. Tang, C. Uher, Multi-Scale Microstructural Thermoelectric Materials: Transport Behavior, Non-Equilibrium Preparation, and Applications, Adv. Mater. 29 (2017) 1602013.

[2] X. Shi, L. Chen, Thermoelectric materials step up, Nat. Mater. 15 (2016) 691-692.

[3] X. Ren, F. Yang, X. Gao, S. Cheng, X. Zhang, H. Dong, W. Hu, Organic Field-Effect Transistor for Energy-Related Applications: Low-Power-Consumption Devices, Near-Infrared Phototransistors, and Organic Thermoelectric Devices, Adv. Energy Mater. 8 (2018) 1801003.

[4] C. Chang, M. Wu, D. He, Y. Pei, C.-F. Wu, X. Wu, H. Yu, F. Zhu, K. Wang, Y. Chen, L. Huang, J.-F. Li, J. He, L.-D. Zhao, 3D charge and 2D phonon transports leading to high out-of-plane ZT in n-type SnSe crystals, Science 360 (2018) 778-783.

[5] J. L. Blackburn, A. J. Ferguson, C. Cho, J. C. Grunlan, Carbon-Nanotube-Based Thermoelectric Materials and Devices, Adv. Mater. 30 (2018) 1704386.

[6] J. Tang, Y. Chen, S. R. McCuskey, L. Chen, G. C. Bazan, Z. Liang, Recent Advances in n‐Type Thermoelectric Nanocomposites, Adv. Electron. Mater. 5 (2019) 1800943.

[7] X. Zhou, Y. Yan, X. Lu, H. Zhu, X. Han, G. Chen, Z. Ren, Routes for high-performance thermoelectric materials, Mater. Today 21 (2018) 974-988.

[8] L. Yang, Z.-G. Chen, M. S. Dargusch, J. Zou, High Performance Thermoelectric Materials: Progress and Their Applications, Adv. Energy Mater. 8 (2018) 1701797.

[9] H. S. Kim, W. Liu, Z. Ren, The bridge between the materials and devices of thermoelectric power generators, Energy Environ. Sci. 10 (2017) 69-85.

[10] V. Vijayakumar, E. Zaborova, L. Biniek, H. Zeng, L. Herrmann, A. Carvalho, O. Boyron, N. Leclerc, M. Brinkmann, Effect of Alkyl Side Chain Length on Doping Kinetics, Thermopower, and Charge Transport Properties in Highly Oriented F4TCNQ-Doped PBTTT Films, ACS Appl. Mater. Interfaces 11 (2019) 4942-4953.

[11] E. W. Zaia, M. P. Gordon, V. Niemann, J. Choi, R. Chatterjee, C. H. Hsu, J. Yano, B. Russ, A. Sahu, J. J. Urban, Molecular Level Insight into Enhanced n‐Type Transport in Solution‐Printed Hybrid Thermoelectrics, Adv. Energy Mater. 9 (2019) 1803469.

[12] Y. Wang, M. Nakano, T. Michinobu, Y. Kiyota, T. Mori, K. Takimiya, Naphthodithiophenediimide–Benzobisthiadiazole-Based Polymers: Versatile n-Type Materials for Field-Effect Transistors and Thermoelectric Devices, Macromolecules 50 (2017) 857-864.

[13] S. Wang, H. Sun, U. Ail, M. Vagin, P. O. Persson, J. W. Andreasen, W. Thiel, M. Berggren, X. Crispin, D. Fazzi, S. Fabiano, Thermoelectric Properties of Solution-Processed n-Doped Ladder-Type Conducting Polymers, Adv. Mater. 28 (2016) 10764-10771.

[14] E. M. Thomas, B. C. Popere, H. Fang, M. L. Chabinyc, R. A. Segalman, Role of Disorder Induced by Doping on the Thermoelectric Properties of Semiconducting Polymers, Chem. Mater. 30 (2018) 2965-2972.

[15] Y. Sun, L. Qiu, L. Tang, H. Geng, H. Wang, F. Zhang, D. Huang, W. Xu, P. Yue, Y. S. Guan, F. Jiao, Y. Sun, D. Tang, C. A. Di, Y. Yi, D. Zhu, Flexible n-Type High-Performance Thermoelectric Thin Films of Poly(nickel-ethylenetetrathiolate) Prepared by an Electrochemical Method, Adv. Mater. 28 (2016) 3351-3358.

[16] E. Lim, K. A. Peterson, G. M. Su, M. L. Chabinyc, Thermoelectric Properties of Poly(3-hexylthiophene) (P3HT) Doped with 2,3,5,6-Tetrafluoro-7,7,8,8-tetracyanoquinodimethane (F4TCNQ) by Vapor-Phase Infiltration, Chem. Mater. 30 (2018) 998-1010.

[17] M. Goel, C. D. Heinrich, G. Krauss, M. Thelakkat, Principles of Structural Design of Conjugated Polymers Showing Excellent Charge Transport toward Thermoelectrics and Bioelectronics Applications, Macromol. Rapid Commun. 40 (2019) 1800915.

[18] G. Zuo, H. Abdalla, M. Kemerink, Conjugated Polymer Blends for Organic Thermoelectrics, Adv. Electron. Mater. 5 (2019) 1800821.

[19] E. W. Zaia, M. P. Gordon, P. Yuan, J. J. Urban, Progress and Perspective: Soft Thermoelectric Materials for Wearable and Internet‐of‐Things Applications, Adv. Electron. Mater. 5 (2019) 1800823.

[20] X. Zhao, D. Madan, Y. Cheng, J. Zhou, H. Li, S. M. Thon, A. E. Bragg, M. E. DeCoster, P. E. Hopkins, H. E. Katz, High Conductivity and Electron-Transfer Validation in an n-Type Fluoride-Anion-Doped Polymer for Thermoelectrics in Air, Adv. Mater. 29 (2017) 1606928.

[21] D. Yuan, D. Huang, C. Zhang, Y. Zou, C. A. Di, X. Zhu, D. Zhu, Efficient Solution-Processed n-Type Small-Molecule Thermoelectric Materials Achieved by Precisely Regulating Energy Level of Organic Dopants, ACS Appl. Mater. Interfaces 9 (2017) 28795-28801.

[22] J. Liu, L. Qiu, G. Portale, M. Koopmans, G. Ten Brink, J. C. Hummelen, L. J. A. Koster, N-Type Organic Thermoelectrics: Improved Power Factor by Tailoring Host-Dopant Miscibility, Adv. Mater. 29 (2017) 1701641.

[23] J. Lee, J. Kim, T. L. Nguyen, M. Kim, J. Park, Y. Lee, S. Hwang, Y.-W. Kwon, J. Kwak, H. Y. Woo, A Planar Cyclopentadithiophene–Benzothiadiazole-Based Copolymer with sp2-Hybridized Bis(alkylsulfanyl)methylene Substituents for Organic Thermoelectric Devices, Macromolecules 51 (2018) 3360-3368.

[24] Y. Chen, M. He, B. Liu, G. C. Bazan, J. Zhou, Z. Liang, Bendable n-Type Metallic Nanocomposites with Large Thermoelectric Power Factor, Adv. Mater. 29 (2017) 1604752.

[25] X. Yin, F. Zhong, Z. Chen, C. Gao, G. Xie, L. Wang, C. Yang, Manipulating the doping level via host-dopant synergism towards high performance n-type thermoelectric composites, Chem. Eng. J. 382 (2020) 122817.

[26] T. Zhu, Y. Liu, C. Fu, J. P. Heremans, J. G. Snyder, X. Zhao, Compromise and Synergy in High-Efficiency Thermoelectric Materials, Adv. Mater. 29 (2017) 1605884.

[27] J. Yang, H.-L. Yip, A. K. Y. Jen, Rational Design of Advanced Thermoelectric Materials, Adv. Energy Mater. 3 (2013) 549-565.

[28] B. Russ, A. Glaudell, J. J. Urban, M. L. Chabinyc, R. A. Segalman, Organic thermoelectric materials for energy harvesting and temperature control, Nat. Rev. Mater. 1 (2016) 16050.

[29] W. Shi, Z. Shuai, D. Wang, Tuning Thermal Transport in Chain-Oriented Conducting Polymers for Enhanced Thermoelectric Efficiency: A Computational Study, Adv. Funct. Mater. 27 (2017) 1702847.

[30] H. Li, E. Plunkett, Z. Cai, B. Qiu, T. Wei, H. Chen, S. M. Thon, D. H. Reich, L. Chen, H. E. Katz, Dopant-Dependent Increase in Seebeck Coefficient and Electrical Conductivity in Blended Polymers with Offset Carrier Energies, Adv. Electron. Mater. 5 (2019) 1800618.

[31] J. Liu, Y. Shi, J. Dong, M. I. Nugraha, X. Qiu, M. Su, R. C. Chiechi, D. Baran, G. Portale, X. Guo, L. J. A. Koster, Overcoming Coulomb Interaction Improves Free-Charge Generation and Thermoelectric Properties for n-Doped Conjugated Polymers, ACS Energy Lett. 4 (2019) 1556-1564.

[32] J. Liu, G. Ye, B. V. Zee, J. Dong, X. Qiu, Y. Liu, G. Portale, R. C. Chiechi, L. J. A. Koster, N-Type Organic Thermoelectrics of Donor-Acceptor Copolymers: Improved Power Factor by Molecular Tailoring of the Density of States, Adv. Mater. 30 (2018) 1804290.

[33] G. Zuo, X. Liu, M. Fahlman, M. Kemerink, High Seebeck Coefficient in Mixtures of Conjugated Polymers, Adv. Funct. Mater. 28 (2018) 1703280.

[34] G. Zuo, Z. Li, E. Wang, M. Kemerink, High Seebeck Coefficient and Power Factor in n-Type Organic Thermoelectrics, Adv. Electron. Mater. 4 (2018) 1700501.

[35] J. Liu, L. Qiu, R. Alessandri, X. Qiu, G. Portale, J. Dong, W. Talsma, G. Ye, A. A. Sengrian, P. C. T. Souza, M. A. Loi, R. C. Chiechi, S. J. Marrink, J. C. Hummelen, L. J. A. Koster, Enhancing Molecular n-Type Doping of Donor-Acceptor Copolymers by Tailoring Side Chains, Adv. Mater. 30 (2018) 1704630.

[36] D. Ju, D. Kim, H. Yook, J. W. Han, K. Cho, Controlling Electrostatic Interaction in PEDOT:PSS to Overcome Thermoelectric Tradeoff Relation, Adv. Funct. Mater. 29 (2019) 1905590.

[37] D. Huang, H. Yao, Y. Cui, Y. Zou, F. Zhang, C. Wang, H. Shen, W. Jin, J. Zhu, Y. Diao, W. Xu, C. A. Di, D. Zhu, Conjugated-Backbone Effect of Organic Small Molecules for n-Type Thermoelectric Materials with ZT over 0.2, J. Am. Chem. Soc. 139 (2017) 13013-13023

[38] K. Shi, F. Zhang, C. A. Di, T. W. Yan, Y. Zou, X. Zhou, D. Zhu, J. Y. Wang, J. Pei, Toward High Performance n-Type Thermoelectric Materials by Rational Modification of BDPPV Backbones, J. Am. Chem. Soc. 137 (2015) 6979-6982.

[39] Y. Xu, H. Sun, A. Liu, H. H. Zhu, W. Li, Y. F. Lin, Y. Y. Noh, Doping: A Key Enabler for Organic Transistors, Adv. Mater. 30 (2018) 1801830.

[40] D. Yuan, Y. Guo, Y. Zeng, Q. Fan, J. Wang, Y. Yi, X. Zhu, Air-Stable n-Type Thermoelectric Materials Enabled by Organic Diradicaloids, Angew. Chem. Int. Ed. 58 (2019) 4958-4962.

[41] X. Yan, M. Xiong, J. T. Li, S. Zhang, Z. Ahmad, Y. Lu, Z. Y. Wang, Z. F. Yao, J. Y. Wang, X. Gu, T. Lei, Pyrazine-Flanked Diketopyrrolopyrrole (DPP): A New Polymer Building Block for High-Performance n-Type Organic Thermoelectrics, J. Am. Chem. Soc. 141 (2019) 20215-20221.

[42] H. Jin, J. Li, J. Iocozzia, X. Zeng, P. C. Wei, C. Yang, N. Li, Z. Liu, J. H. He, T. Zhu, J. Wang, Z. Lin, S. Wang, Hybrid Organic-Inorganic Thermoelectric Materials and Devices, Angew. Chem. Int. Ed. 58 (2019) 15206-15226.

[43] U. Ail, M. J. Jafari, H. Wang, T. Ederth, M. Berggren, X. Crispin, Thermoelectric Properties of Polymeric Mixed Conductors, Adv. Funct. Mater. 26 (2016) 6288-6296.

[44] H. Wang, U. Ail, R. Gabrielsson, M. Berggren, X. Crispin, Ionic Seebeck Effect in Conducting Polymers, Adv. Energy Mater. 5 (2015) 1500044.

[45] W. B. Chang, C. M. Evans, B. C. Popere, B. M. Russ, J. Liu, J. Newman, R. A. Segalman, Harvesting Waste Heat in Unipolar Ion Conducting Polymers, ACS Macro Letters 5 (2015) 94-98.

[46] D. Zhao, H. Wang, Z. U. Khan, J. C. Chen, R. Gabrielsson, M. P. Jonsson, M. Berggren, X. Crispin, Ionic thermoelectric supercapacitors, Energy Environ. Sci. 9 (2016) 1450-1457.

[47] F. Jiao, A. Naderi, D. Zhao, J. Schlueter, M. Shahi, J. Sundström, H. Granberg, J. Edberg, U. Ail, J. Brill, T. Lindström, M. Berggren, X. Crispin, Ionic thermoelectric paper, J. Mater. Chem. A. 5 (2017) 16883-16888.

[48] R. F. Stout, A. S. Khair, Diffuse charge dynamics in ionic thermoelectrochemical systems, Phys Rev E 96 (2017) 022604.

[49] X. Guan, H. Cheng, J. Ouyang, Significant enhancement in the Seebeck coefficient and power factor of thermoelectric polymers by the Soret effect of polyelectrolytes, J. Mater. Chem. A. 6 (2018) 19347-19352.

[50] A. de Izarra, S. Park, J. Lee, Y. Lansac, Y. H. Jang, Ionic Liquid Designed for PEDOT:PSS Conductivity Enhancement, J. Am. Chem. Soc. 140 (2018) 5375-5384.

[51] N. Saxena, B. Pretzl, X. Lamprecht, L. Biessmann, D. Yang, N. Li, C. Bilko, S. Bernstorff, P. Muller-Buschbaum, Ionic Liquids as Post-Treatment Agents for Simultaneous Improvement of Seebeck Coefficient and Electrical Conductivity in PEDOT:PSS Films, ACS Appl. Mater. Interfaces 11 (2019) 8060-8071.

[52] Z. Fan, D. Du, X. Guan, J. Ouyang, Polymer films with ultrahigh thermoelectric properties arising from significant seebeck coefficient enhancement by ion accumulation on surface, Nano Energy 51 (2018) 481-488.

[53] K. Choi, S. L. Kim, S. I. Yi, J. H. Hsu, C. Yu, Promoting Dual Electronic and Ionic Transport in PEDOT by Embedding Carbon Nanotubes for Large Thermoelectric Responses, ACS Appl. Mater. Interfaces 10 (2018) 23891-23899.

[54] Z. Fan, J. Ouyang, Thermoelectric Properties of PEDOT:PSS, Adv. Electron. Mater. 5 (2019) 1800769.

[55] H. Cheng, X. He, Z. Fan, J. Ouyang, Flexible Quasi‐Solid State Ionogels with Remarkable Seebeck Coefficient and High Thermoelectric Properties, Adv. Energy Mater. 9 (2019) 1901085.

[56] T. J. Abraham, D. R. MacFarlane, J. M. Pringle, High Seebeck coefficient redox ionic liquid electrolytes for thermal energy harvesting, Energy Environ. Sci. 6 (2013) 2639.

[57] S. Motaghiani, K. Mirabbaszadeh, Density functional study of platinum polyyne monomer, oligomer, and polymer: Ground state geometrical and electronic structures, Int. J. Quantum Chem. 113 (2013) 1650-1659.

[58] W. Shi, D. Wang, Z. Shuai, High‐Performance Organic Thermoelectric Materials: Theoretical Insights and Computational Design, Adv. Electron. Mater. 5 (2019) 1800882.

[59] W. Y. Wong, X. Z. Wang, Z. He, A. B. Djurisic, C. T. Yip, K. Y. Cheung, H. Wang, C. S. Mak, W. K. Chan, Metallated conjugated polymers as a new avenue towards high-efficiency polymer solar cells, Nat. Mater. 6 (2007) 521-527.

[60] X. Yin, X. Liu, Y. Peng, W. Zeng, C. Zhong, G. Xie, L. Wang, J. Fang, C. Yang, Multichannel Strategies to Produce Stabilized Azaphenalene Diradicals: A Predictable Model to Generate Self-Doped Cathode Interfacial Layers for Organic Photovoltaics, Adv. Funct. Mater. 29 (2019) 1806125.

[61] X. Yin, G. Xie, Y. Peng, B. Wang, T. Chen, S. Li, W. Zhang, L. Wang, C. Yang, Self-Doping Cathode Interfacial Material Simultaneously Enabling High Electron Mobility and Powerful Work Function Tunability for High-Efficiency All-Solution-Processed Polymer Light-Emitting Diodes, Adv. Funct. Mater. 27 (2017) 1700695.

[62] H. Wang, J. H. Hsu, S. I. Yi, S. L. Kim, K. Choi, G. Yang, C. Yu, Thermally Driven Large N-Type Voltage Responses from Hybrids of Carbon Nanotubes and Poly(3,4-ethylenedioxythiophene) with Tetrakis(dimethylamino)ethylene, Adv. Mater. 27 (2015) 6855-6861.

[63] A. Malti, J. Edberg, H. Granberg, Z. U. Khan, J. W. Andreasen, X. Liu, D. Zhao, H. Zhang, Y. Yao, J. W. Brill, I. Engquist, M. Fahlman, L. Wagberg, X. Crispin, M. Berggren, An Organic Mixed Ion-Electron Conductor for Power Electronics, Adv. Sci. 3 (2016) 1500305.

[64] H. Wang, D. Zhao, Z. U. Khan, S. Puzinas, M. P. Jonsson, M. Berggren, X. Crispin, Ionic Thermoelectric Figure of Merit for Charging of Supercapacitors, Adv. Electron. Mater. 3 (2017) 1700013.

[65] J. P. Heremans, V. Jovovic, E. S. Toberer, A. Saramat, K. Kurosaki, A. Charoenphakdee, S. Yamanaka, G. J. Snyder, Enhancement of Thermoelectric Efficiency in PbTe by Distortion of the Electronic Density of States, Science 321 (2008) 554-557.

[66] B. Delley, From molecules to solids with the DMol3 approach, J. Chem. Phys. 113 (2000) 7756-7764.

[67] C. Gao, Y. Liu, Y. Gao, Y. Zhou, X. Zhou, X. Yin, C. Pan, C. Yang, H. Wang, G. Chen, L. Wang, High-performance n-type thermoelectric composites of acridones with tethered tertiary amines and carbon nanotubes, J. Mater. Chem. A. 6 (2018) 20161-20169.